ELSEVIER

Polymer 42 (2001) 6515–6526

polymer

www.elsevier.nl/locate/polymer

Organic short fibre/thermoplastic composites: morphology and thermorheological analysis

M.-F. Boyaud[a], A. Aït-Kadi[a,*], M. Bousmina[a], A. Michel[b], Ph. Cassagnau[b]

[a]*Department of Chemical Engineering, CERSIM, Laval University, Sainte-Foy, Qué., Canada G1K 7P4*

[b]*Laboratoire des Matériaux Plastiques et Biomatériaux, UMR 5627, Bâtiment 69 303, Université Claude-Bernard Lyon 1, 43 Bvd du 11 Novembre 1918, ISTIL 622 Villeurbanne Cédex, France*

Received 9 February 2000; received in revised form 6 November 2000; accepted 9 November 2000

Abstract

A study to evaluate the thermorheological properties of organic in situ composites with short polymer fibres dispersed in a thermoplastic matrix has been carried out. High-density polyethylene/Poly(butylene terephtalate) HDPE/PBT, HDPE/EVA-9/PBT and HDPE/(EVA-9-Bu_2SnO)/PBT (in situ compatibilised blends) were melt blended in a twin-screw extruder, drawn at the die exit and cooled. Morphological results revealed that it is possible to generate fibrillar morphologies for high PBT concentration and draw ratios higher than 1. Compatibilisation with in situ generated PBT-g-EVA-9 compatibiliser was achieved. Rheological properties in the melt state and in the solid state were used to analyse the compatibilisation and the reinforcing effect of fibrils. Two phenomenological models, Takayanagi and Halpin-Tsaï, were used to describe the variations of E' and tan δ as a function of temperature. © 2001 Published by Elsevier Science Ltd.

Keywords: In situ composites; Immiscible blends; Thermorheology

1. Introduction

Combining materials with different characteristics to enlarge the spectrum of properties of the final material has been used for years. Blending and alloying of immiscible polymer blends, as well as incorporating solid substrates in polymeric matrices to make composite materials, are among the possibilities made available to scientists and engineers working in the area of polymeric materials. The approach presented here is a combination of both alloying two immiscible polymers and making a short fibre thermoplastic composite. The materials obtained in this way are called in situ *organic thermoplastic composites*.

Different approaches were developed to obtain these types of material. Each of them corresponds to a specific process and to a specific size of the reinforcing constituent. One of these approaches consists in melt blending a liquid crystalline polymer (LCP) with a thermoplastic matrix (molecular composite) [1,2]. Chinsirikul et al. [3] and La Mantia et al. [4] showed that the addition of LCP increases tensile modulus of polyethylene matrices. The dispersed LCP phase is easily orientable into fibrils due to its molecular structure [5–7]. Magagnini et al. [8] worked on the compatibilisation of PE/LCP blends. They showed that it is possible to generate a PE-g-LCP copolymer at the interface in order to improve adhesion between the phases, thereby improving the mechanical properties. It was shown by Wong et al. [9], Mehta and Deopura [10], Sabol et al. [11] and Heino [12] that thermoplastic/LCP blends have indeed improved mechanical properties. However, preparation steps generally require high temperatures that often lead to thermal degradation of one or both components of the blend [13].

Another approach consists in the production of microfibrillar-reinforced composites (MFC). These rod-like composites are processed in two steps: extrusion and drawing of the blends, followed by annealing at a temperature below the melting point of at least one of the components. The result is the melting of the lower-melting constituent which will play later the role of the matrix in the final composite [14]. This approach can also be used with reactive polymers to generate copolymers in one of the above steps of the process. The generated copolymer layer is expected to enhance interactions and gradually change the final morphology [15,16]. An important feature of MFCs is that they show large deformability as well as mechanical properties comparable to those of glass-fibre reinforced materials, (see for example Fakirov et al. [17] and Apostolov et al. [18] in the case of nylon composites. However, the MFC approach can only be applied to very specific polymer blends: blending temperature of the two

* Corresponding author. Tel.: +1-418-656-3375; fax: +1-418-656-5993.
E-mail address: aitkadi@gch.ulaval.ca (A. Aït-Kadi).

0032-3861/01/$ - see front matter © 2001 Published by Elsevier Science Ltd.
PII: S0032-3861(00)00878-8

constituents must be low enough to avoid thermal degradation of the low melting temperature component. This component must have a relatively low melting temperature compared to the other constituent in order to offer a large enough temperature window for processing. This may limit the choice of polymer pairs to be used with this approach.

Li et al. [19] worked on polypropylene/polyamide-6 (PP/PA) in situ composites and showed fibrillation of the PA dispersed phase into the matrix. However, the processability of their final anisotropic material happened to be of limited usefulness.

A more versatile way of processing in situ composites has recently been developed by Monticciollo et al. [20] for high-density polyethylene/poly(butylene terephtalate) (HDPE/PBT) system and applied to polypropylene/polyamide (PP/PA) system by Pesneau et al. [21,22]. The resulting material was found to behave as a true composite. The second step is a reprocessing of the pellets, e.g. by injection moulding, at a temperature below the melting temperature of the dispersed fibrillar phase.

From the thermodynamic point of view, most polymer blends are immiscible. For a better stress transfer between the phases and for each constituent to play its role in an efficient way, the two components must be compatibilised. Copolymers are generally used to achieve compatibilisation between immiscible polymer blends. These third components are either mechanically added to the basic constituents using a specific experimental protocol or else chemically generated in situ during one or the other steps of the composite preparation. The former approach is well documented and has been successfully used for a variety of immiscible polymer blends [23]. The other approach can be used for example with reactive extrusion, a process particularly suitable for the two-step in situ composites [24,25].

The aim of the present work is to produce organic composites with short polymer fibres dispersed in situ in a thermoplastic matrix. The tow-phase blends are made of HDPE as a matrix and PBT as a dispersed phase.

The compatibilisation procedure was developed by Pesneau et al. [26] who studied the transesterification reactions for the generation of PBT-g-EVA copolymer during reactive extrusion. According to the work of Legros et al. [27], the PBT/PE/EVA system, combined with the transesterification precursor Bu_2SnO leads to the formation of PBT/EVA copolymer which acts as a compatibiliser between the immiscible HDPE matrix and the PBT dispersed phase. The effect of this type of compatibiliser on the morphology and the thermorheological properties of the generated organic composites will be presented.

2. Experimental

2.1. Material

HDPE (Finathene 3802, density = 938 kg m^{-3}) was supplied by Fina. It has a melting temperature of 130°C. The poly(ethylene-co-vinyl acetate) (EVA-9, Evatane 1020 VN3, density = 929 kg m^{-3}) was supplied by Elf-Atochem. It has 9% by weight acetate groups (CH_3COO–) and melts at 98°C. This copolymer is completely miscible with HDPE [28]. Poly(butylene terephtalate) (PBT, Crastin S600, density = 1310 kg m^{-3}), a product from DuPont, melts at 225°C. In order to minimise hydrolysis in the melt during processing, PBT was dried at 80°C and EVA-9 at 40°C under vacuum during 4 h. The dibutyltin oxide (Bu_2SnO) compatibilising catalyst was obtained from Aldrich. It is active at temperatures higher than 180°C. In all reactive blends, Bu_2SnO concentration was fixed at 0.5 wt% (based on the total weight of the blend). All the blends containing EVA-9 are based on a mixture of 80 wt% of HDPE and 20 wt% of EVA-9 (80/20 wt% HDPE/EVA-9). The blend compositions are all expressed in terms of weight percentage throughout the paper.

2.2. Processing operations

During the first step of the in situ composite process, blends of HDPE/PBT, HDPE/EVA-9/PBT and HDPE/(EVA-9-Bu_2SnO)/PBT with various concentrations of PBT (10, 20, 30 and 40%) were extruded using a Leistritz LSM-30-34 co-rotating twin-screw extruder with a length to diameter ratio, L/D, of 35. The temperature profile in the extruder was 200–225–250–250°C (the last one corresponding to the die temperature), the screw rotation speed, N, was set at 160 rpm and the extrudate mass flow rate, Q, at 5 kg h^{-1}. For the reactive blends, a pre-extrusion at 150°C, $N = 100$ rpm and $Q = 7$ kg h^{-1} of EVA-9-Bu_2SnO was performed for safety reasons and to diminish hydrolysis during transesterification reactions. The extruder was equipped with three 1.5 mm diameter capillary dies, which leads to an apparent shear rate ($\dot{\gamma}_A$) of 2104 s^{-1}. At the die exit, the molten extrudate was drawn by two calendar rolls of a laboratory stretcher, placed at a distance $\Delta l = 0.15$ m from the die. The draw ratio, λ, defined as V_r/V_e, where V_r is the linear velocity of the rolls and V_e the linear velocity of the extrudate, can be adjusted by changing the speed of the calendar rolls. An elongational rate can be defined as $\dot{\epsilon} = (V_r - V_e)/\Delta l$. Two different apparent extensional rates of 1.75 s^{-1} and 4.37 s^{-1}, were obtained for $\lambda = 2$ and 3.5, respectively. The fibrillation, caused by phase deformation, takes place during the drawing operation. After the drawing step, the extrudate is water-quenched, in order to freeze the morphology, chopped and dried. For comparison purposes, HDPE/EVA-9/PBT without a Bu_2SnO catalyst was also studied in order to evaluate possible changes caused by the sole presence of EVA-9 on the HDPE matrix and its effect on the final properties of the composite.

2.3. Reactive extrusion

While using a catalyst, an extruder can become a

chemical reactor where copolymerisation reactions can take place between two polymers as reactants. The use of this process gives a homogeneous mixing and temperature, and allows an easier control of the operation pressure [29,30]. It is, however, necessary to have a good estimate of the residence time of the polymer reactants in the extruder and to be sure that it will be compatible with the system reactions kinetics. In this work, the residence time in the extruder, for the previously given N and Q, is approximately 160 s, and it is found to be sufficient since the transesterification reactions are relatively fast at 250°C [28]. According to Bonetti [31], Bu_2SnO reacts with the acetate groups of the EVA-9 to generate distannoxanes. These intermediate components are good catalysts for the redistributive transesterification reactions between PBT ester functions and those of the EVA-9. These reactions were well studied by Espinasse et al. [32]. Pesneau et al. [26] have shown that addition of 1% of Bu_2SnO in binary blends effectively enables synthesis of the PBT-g-EVA copolymers.

2.4. NMR analysis

Liquid proton nuclear magnetic resonance (^{1}H-NMR) spectroscopy was carried out on a Bruker AC-300 apparatus at 300 MHz in a $CF_3COOD + CDCl_3$ (1/1 by volume) solution. Chemical shifts (δ) are given in ppm in reference to tetramethylsilane (TMS).

2.5. Morphology

Morphology of the blends was examined by scanning electron microscopy (JEOL JSM 840A). The samples were cryofractured in liquid nitrogen and vacuum metallised before analysis. The drawn samples were fractured in both transversal and longitudinal directions relative to the flow and drawing directions at the die exit, in order to evaluate the aspect ratio of the PBT phase after deformation.

2.6. Thermorheological properties

The rheological properties in the molten state were carried out on a rotational rheometer (ARES, Rheometric Scientific), using 25 mm diameter parallel plates. A time sweep was performed on the HDPE/(EVA-9-Bu_2SnO)/PBT 30% PBT composite at 180°C and 1 rad s^{-1} to determine the thermal stability time of the reactive samples. No changes were reported for up to 100 min, indicating no thermal degradation will occur during the rheological measurements. Strain sweep tests were performed in order to determine the linear viscoelasticity domain. Frequency sweep tests from 0.01 to 100 rad s^{-1} were then performed at 180°C and 0.5% strain. In the solid state, analyses were performed on a Rheometric Solid Analyser (RSA-II, Rheometric Scientific) using a dual cantilever geometry. Sample dimensions were $L \times l \times w = 6.0 \times 4.5 \times 1.5$ mm. Temperature sweep tests (from −150 to 250°C) were all carried out at a frequency of 1 rad s^{-1}.

3. Results and discussion

3.1. Morphology

Extrusion and post extrusion of the melt blend are the critical steps for the in situ composite process. In this part of the process, dispersion and orientation of the minor phase (PBT) to be frozen in the final composite is generated. As often cited in the literature, blend morphology depends strongly on the rheological properties of each polymer, interfacial tension and processing parameter. The particle dispersion is optimum when the viscosity ratio is close to 1 [33]. Also, the morphology is more dependent on the flow in the die than on the screw speed or on the volumetric flow rate for the present extrusion procedure. Blend composition is another important parameter. All the blends with PBT concentration ranging from 10% to 30% that have undergone a draw ratio 1%, as shown in Fig. 1 for the 70/30 blend, show a nodular morphology, even though there is a strong shear flow in the die. Systems containing 40% PBT were found to have a co-continuous morphology (see Fig. 2). Similar results were obtained earlier by Pesneau [28]. No results will be reported on these particular systems (40% PBT) since they were not easy to process.

Table 1 gives the mean diameter of the minor phase as a function of the blend composition for a draw ratio of 2. The results show that a slight increase of the diameter of the minor phase is observed when PBT concentration increases from 10 to 20%. This observation is attributed to coalescence phenomena. Upon increase PBT concentration from 20 to 30%, a slight decrease of the fibre diameter is then observed. The decrease here can be attributed to the fragmentation phenomenon and Rayleigh instabilities due to relatively large aspect ratios that can be reached during the drawing process. The results of Table 1 also indicate that at

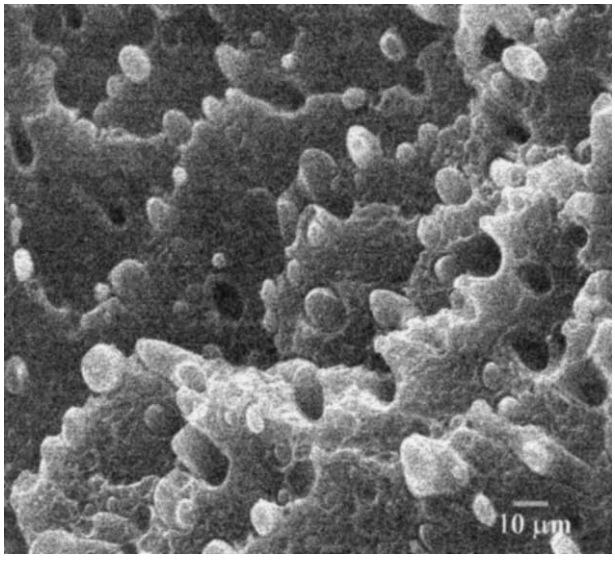

Fig. 1. Micrography of HDPE/PBT — 70/30 composite for a draw ratio $\lambda = 1$ (nodular morphology); 2000×.

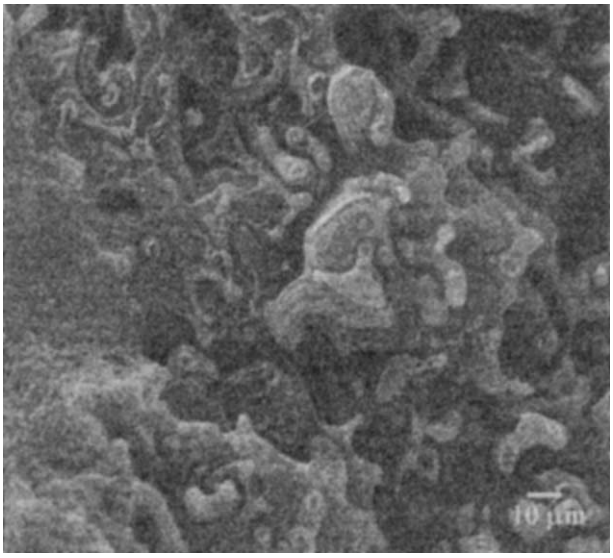

Fig. 2. Micrography of HDPE/PBT — 60/40 composite for a draw ratio $\lambda = 2$ (co-continuous morphology); 2000×.

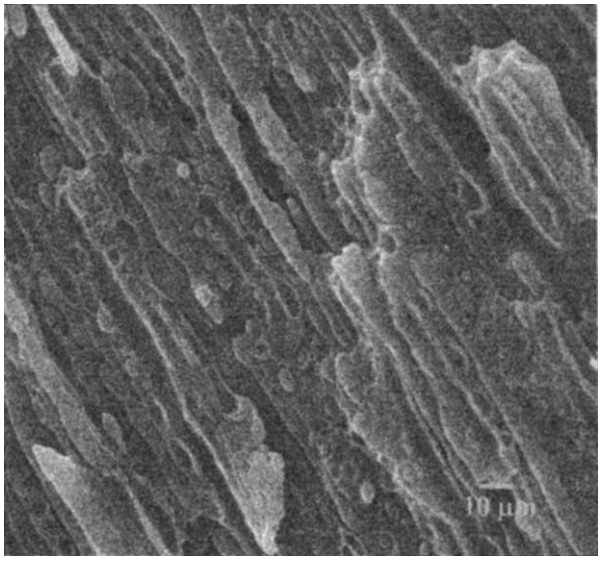

Fig. 3. Morphology of HDPE/PBT — 70/30 composite for $\lambda = 1$; 2000×.

10% PBT content, the droplets remain spherical. However, for 20 and 30% blends, fibre length increases upon increasing PBT concentration. The same observation can be made for samples containing EVA-9. Samples containing EVA-9 composites are found to have higher fibrils length as compared to those without EVA-9. In all cases (with and without EVA-9) the aspect ratio increases when the PBT concentration increases from 20 to 30% and remains equal to one for the 10% PBT blends.

The effect of draw ratio is shown in Table 2. The results are shown only for the 30% PBT for the sake of brevity. They indicate that the morphology is mainly nodular with only few fibrils (mostly generated by the shear flow at the wall of the die), when the draw ratio is equal to 1 (see Fig. 3). When the draw ratio is increased (see Fig. 4, for $\lambda = 2$) fibrils are formed. It is worth noting that in the case of the blend without EVA-9 and for $\lambda = 3.5$, the fibre diameter increases the length and the aspect ratio decrease as compared to the results obtained for $\lambda = 2$ (see Table 2). This is attributed to the fragmentation phenomenon, which becomes important when the draw ratio increases. The equivalent results obtained for the EVA-9 containing composites are also shown in Table 2. In this case, higher fibre lengths and aspect ratios are achieved. The fragmentation phenomenon does not seem to be important at $\lambda = 3.5$ for this particular system.

The presence of PBT-g-EVA-9 copolymer, generated by adding the transesterification precursor Bu_2SnO to the system, results in an appreciable decrease in both PBT fibre diameter and length as well as the aspect ratio (see Table 2 for $\lambda = 2$). This is attributed to the fact that small droplets are generally more difficult to deform than larger ones [34]. Reduction in particle dimensions is due to several parameters including a decrease in the interfacial tension, generally observed upon addition of copolymers; enhanced interphase interactions and stabilisation of the morphology as a consequence of a decrease in the coalescence phenomena. Fig. 5 shows the nodular morphology ($\lambda = 1$) obtained for a 30% PBT composite, which indicates the strong decrease in nodule diameters as compared to the equivalent results shown in Fig. 1. As the interfacial tension decreases, the interphase contrast diminishes in a clearly visible way (see Fig. 5).

To assess the presence of PBT-g-EVA-9, an extraction strategy, based on the work of Pesneau et al. [26], has been performed. This approach was necessary due to the fact that the copolymer represents only a very small fraction of the overall system. The first extraction consists of dissolving PBT in dichloro acetic acid (DCAA). The second one was carried out with hot xylene using a Soxhlet apparatus to extract the HDPE and HDPE/EVA-9 matrix. Finally, in a third step, tetrachloroethane was used to separate impurities and reticulated components from the grafted PBT. ^{1}H-NMR

Table 1
Diameter, length and aspect ratio for in situ composites at a draw ratio $\lambda = 2$

Sample composition: HDPE/EVA-9/PBT	72/18/10	90/00/10	64/16/20	80/00/20	56/14/30	70/00/30
Diameter (µm)	1.85	1.38	1.89	1.79	1.40	1.40
Length (µm)	1	1	70.80	63.90	88.50	73.80
Aspect ratio	1	1	37	36	63	53

Table 2
Effect of draw ratio (λ) on diameter, length and aspect ratio of the 30% PBT composites

Sample composition: HDPE/(EVA-9-Bu_2SnO)/PBT	56/(14-0)/30	70/(00-0)/30	56/(14-0)/30	70/(00-0)/30	56/(14-0)/30	70/(0-0)/30	56/(13.5-0.5)/30
Draw ratio, λ	1		2		3.5		2
Diameter (μm)	4.00	5.92	1.40	1.40	1.24	2.01	1.13
Length μm)	1	1	88.50	73.80	91.70	66.30	45.60
Aspect ratio	1	1	63	53	74	33	40

Table 3
^{1}H-NMR peaks and chemical shifts (δ) of extracted PBT-g-EVA-9

Peaks	δ (ppm)[a]
PBT	8.150 (a), 4.500 (b), 2.025 (c)
PBT terminated by CH_3COO–	3.915 (d)
CH_3CO, from initial EVA-9	2.155 (e)
CH α (CH_3COO- attached)	4.670
CH α' (grafted PBT)	4.930
CH_2 β (CH α- attached)	1.570
CH_2 β' (CH α'- attached)	1.715
$(CH_2)_n$	1.270 (f)

[a] Letters refer to Fig. 6.

spectrum of the PBT-g-EVA-9, extracted from the 56/(13.5-0.5)/30 sample, is shown in Fig. 6. The peaks of the spectrum, listed in Table 3, refer to the presence of PBT-g-EVA-9. The characteristic peaks are associated with CHα' (4.930 ppm peak) and $CH_2\beta'$ (1.715 ppm peak) [26].

3.2. Thermorheological properties

The different composites were analysed in molten and solid state by Dynamic Mechanical Analysis (DMA). Frequency sweeps were performed on each sample at 180°C in order to keep the matrix in the molten state and the dispersed phase in the solid state. Fig. 7 shows the effect of PBT concentration on the storage modulus (G') for non-drawn composites with HDPE matrix ($\lambda = 1$; drawing refers to the first step of the preparation of the composite). The presence of PBT results in an increase of G' over the whole range of frequencies (10^{-2}–10^2 rad s^{-1}). Moreover, for the 30% PBT composite, a pseudo equilibrium plateau modulus is observed in the low frequency region. These results confirm those obtained by Monticciolo et al. [20] on HDPE/PBT organic composites. This pseudo equilibrium plateau is attributed to interparticular interactions. Similar behaviour was observed with several multiphase systems (rubber modified polymer melts: Moroni and Casale [35], Münstedt [36], Aoki [37], Bousmina and Müller [38,39], Carreau et al. [40]; particulate suspensions and composites: Aranguren et al. [41], Otsubo [42]). This plateau modulus is found to depend on particle content, the molecular weight of the matrix as well as the degree of dispersion of particles in the system [40]. The magnitude of the plateau is also found to correlate with the surface distance between neighbouring particles. The shorter the interparticular distance, the stronger is the interaction between the particles and the higher is the pseudo equilibrium modulus [38,39]. Aoki and Nakayama [43] also

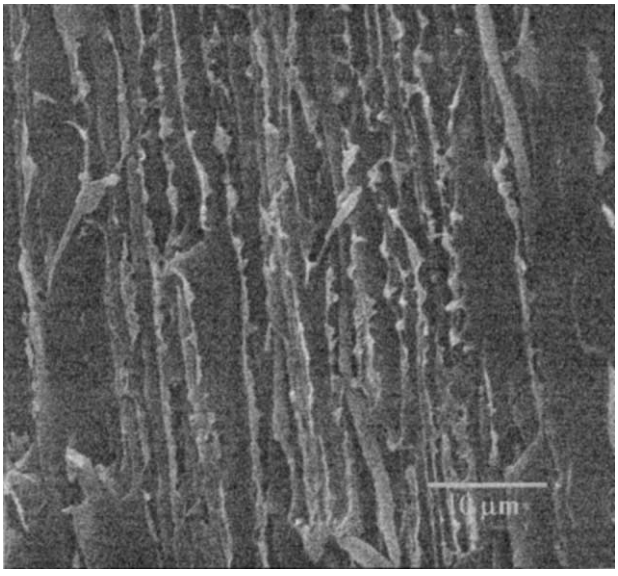

Fig. 4. Morphology of HDPE/PBT — 70/30 composite for $\lambda = 2$; 2000×.

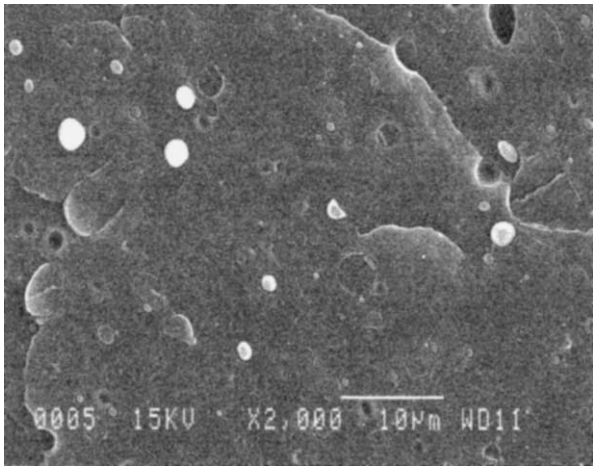

Fig. 5. Morphology of PEHD/(EVA-9-Bu_2SnO)/PBT — 56/(13.5-0.5)/30 for $\lambda = 1$; 2000×.

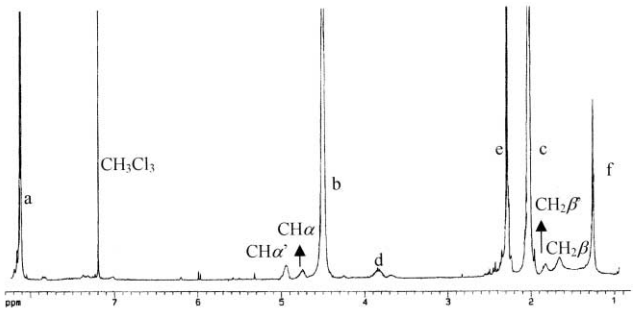

Fig. 6. ^{1}H-NMR spectrum (300 MHz) in $CF_3COOD + CDCl_3$ (1/1 by volume) of the extracted PBT-g-EVA-9 copolymer.

found that the relaxation spectra calculated using the Tschoegl equation [44] correlate with the surface distance between neighbouring particles and rubber volume fraction for ABS resins. The spectra became higher as the particle content increases and the particle size decreases [43]. Using blends containing the same amount of rubber particles but with different degrees of dispersion, Bousmina and Muller [38,39] showed that the plateau modulus is related to the percolation phenomenon that occurs for particles with uniform size at around 16 vol.% dispersion. Our results show that this plateau is not observed with the 10 and 20% PBT composites at least in the explored frequency range.

The presence of EVA-9 in the matrix results in an important increase in the storage modulus for the 30% PBT concentration composite. As shown in Fig. 8, the plateau modulus is almost three times higher for the 30% PBT samples with an HDPE/EVA-9 matrix, and $\lambda = 1$, as compared to the one without EVA-9. For 10 and 20% PBT concentrations, the presence of the EVA-9 does not strongly affect the storage modulus. The increase of the pseudo

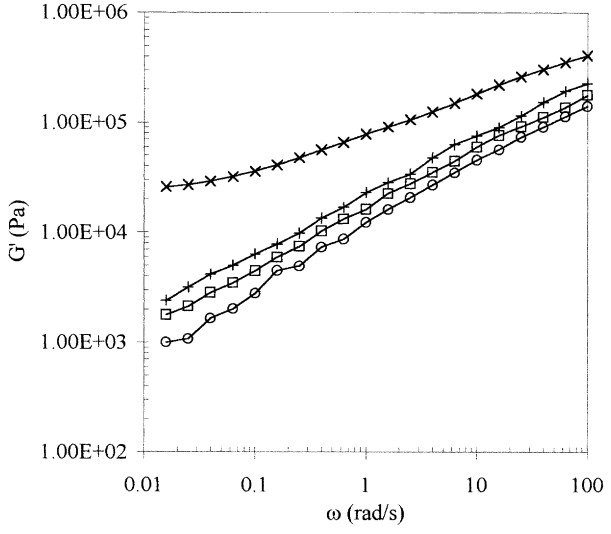

Fig. 7. Storage modulus of HDPE/PBT samples for $\lambda = 1$: HDPE alone (○), with 10% PBT (□), 20% PBT (+) and 30% PBT (X) —$T = 180$°C.

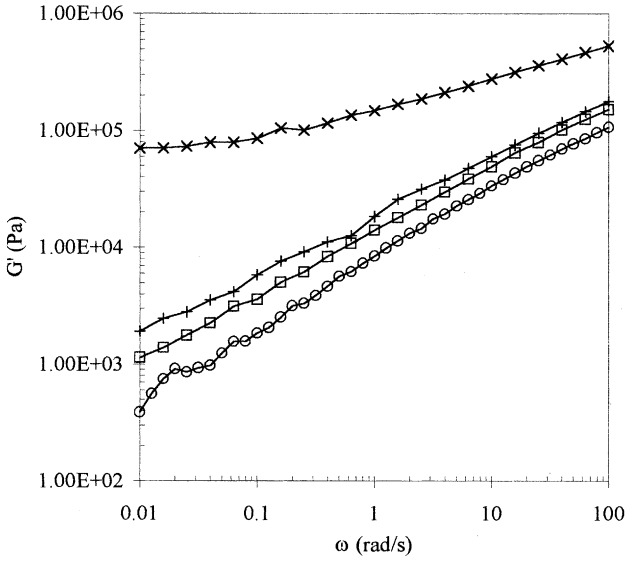

Fig. 8. Storage modulus of HDPE/EVA-9/PBT samples for $\lambda = 1$: HDPE/EVA-9 alone (○), with 10% PBT (□), 20% PBT (+), 30% PBT (X) — $T = 180$°C.

equilibrium modulus is attributed to the decrease of the particle diameter in the presence of EVA-9 (see Table 2), which in turn is attributed to a decrease in the interfacial tension between the components. Legros et al. [27], have determined interfacial tension for different HDPE/EVA-28/PBT system. As shown in Table 4, the interfacial tension of HDPE/PBT system is higher than that of EVA-28/PBT.

In the presence of Bu_2SnO (see Fig. 9) the storage modulus for samples with nodular morphology is found to be slightly higher than that of HDPE/PBT and HDPE/EVA-9/PBT blends without catalyst. The effect of compatibilisation

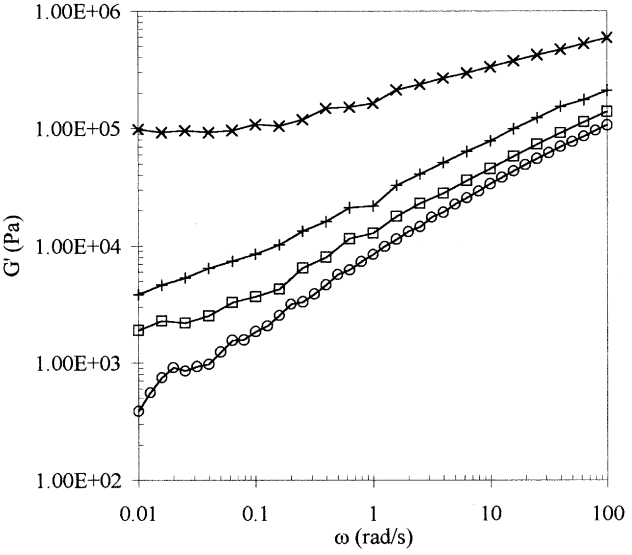

Fig. 9. Storage modulus of HDPE/(EVA-9-Bu_2SnO)/PBT samples for $\lambda = 1$: HDPE/EVA-9 (○), 10% PBT (□), 20% PBT (+), 30% PBT (X) —$T = 180$°C.

Table 4
Interfacial tension (ν) of selected blends (Legros et al. [27])

Interfaces	HDPE/PBT	EVA-28/PBT	HDPE/EVA-28
ν (mN m^{-1})	10.4	6.2	2.5

is found to be more pronounced in the case of elongational viscosity as reported recently by Boyaud et al. [45] for EVA/PBT composites. With the compatibiliser, the modulus for the 10 and the 20% PBT composites slightly increases but only in the low frequency region, where it shows a tendency to level off. It is not clear, however, whether these composites also reach a pseudo equilibrium plateau, the frequency range explored here being rather limited. The slightly higher values of G' obtained in the presence of Bu_2SnO can be attributed to the slight decrease in particle diameter (see Table 2) as well as to an increase of interactions between the components due to the formation of PBT-g-EVA-9 copolymer, as assessed by ^{1}H-NMR results given in Fig. 6 and Table 3. Moreover, when the PBT concentration decreases, the amount of generated copolymer decreases and the compatibility effect is less pronounced thereby reducing its possible effect on rheological properties.

Fig. 10 shows the results of the storage modulus for the 30% PBT composites at different draw ratios. The results clearly indicate that the storage modulus is higher for the drawn composites. The increase is again more pronounced in the low frequency region, where long-range contributions are taken into account. In the high frequency region the draw ratio has only a slight effect. The results of Fig. 10 also show that the G' values are lower for $\lambda = 3.5$ as compared to the result obtained for $\lambda = 2$. This is attributed to the smaller PBT fibre aspect ratio observed for higher draw ratios (see also Table 2 for the 70/30 HDPE/PBT

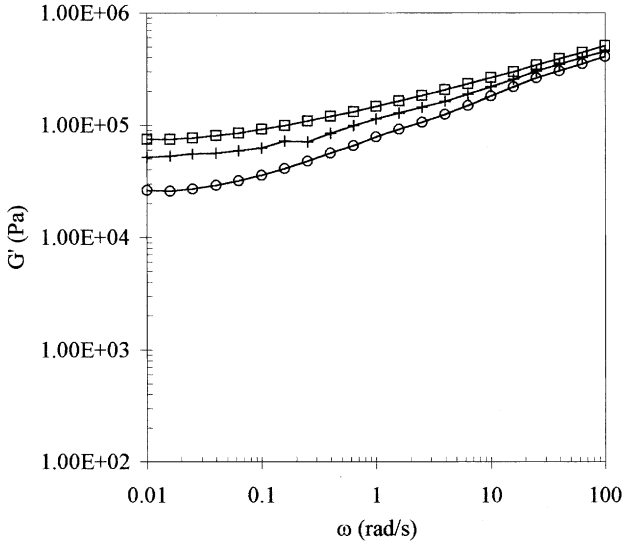

Fig. 10. Effect of draw ratio, λ on the storage modulus of HDPE/PBT — 70/30 samples: $\lambda = 1$ (○), $\lambda = 2$ (□), $\lambda = 3.5$ (+).

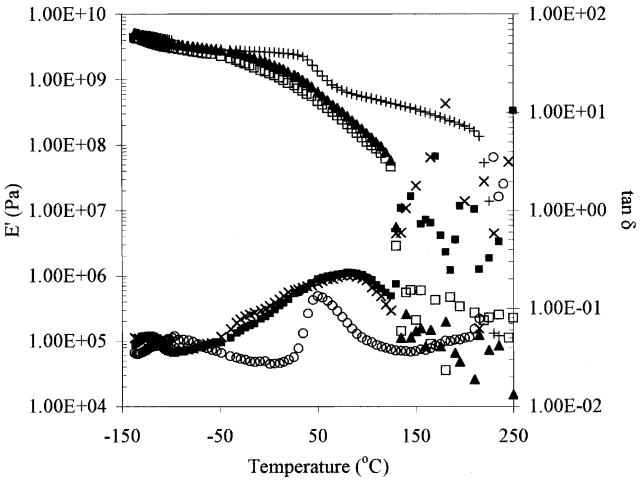

Fig. 11. Effect of temperature on dynamic mechanical properties of pure polymers: PBT (E' (+), tan δ (○); HDPE (E'(▲), tan δ (□)); HDPE/EVA-9 (E' (□), tan δ (X)).

composite). The higher pseudo-equilibrium plateau observed with anisometric particles is attributed to the smaller inter-particle distance and hence to stronger particle–particle interactions. Equivalent results were obtained by Monticciolo et al. [20] for HDPE/PBT composites

For the dynamic mechanical and thermal analysis (DMTA), the effects of PBT concentration, draw ratio and compatibilisation were investigated. Temperature sweeps were performed on the different composites from −150 to 250°C. Fig. 11 shows the different transitions obtained for HDPE, HDPE/EVA-9 and PBT. The different transitions observed at the maxima of tan δ are attributed to the α transition of the crystalline phase of HDPE for the transition at 91°C (see Fig. 11). In the presence of EVA-9, this transition remains unchanged. α transition of EVA-9 is however observed at 22°C. The transition at −17°C is attributed to the branched structure of the EVA-9 [28]. The transition at 50°C in the tan δ curve of PBT corresponds to the glass transition. The melting temperature of HDPE and HDPE/EVA-9 are found to be the same (around 130°C) and the melting temperature of PBT is close to 225°C. These results are in accordance with those generally reported in the literature and those reported by Pesneau [28]. The presence of EVA-9 in the HDPE matrix results in a slight decrease of the modulus below the melt temperature.

Fig. 12 presents the results of storage modulus (E') as a function of temperature for different PBT concentrations at $\lambda = 2$. The results indicate that below the melting temperature of the matrix, there is no appreciable effect of PBT on the storage modulus of the composites. Above the melting temperature of HDPE, and below that of PBT, an increase in E' is observed upon increasing the PBT concentration. In this temperature range, the system behaves like a suspension of a solid substrate (PBT particles or fibrils) in a viscoelastic medium. It is then expected to see an increase of the storage

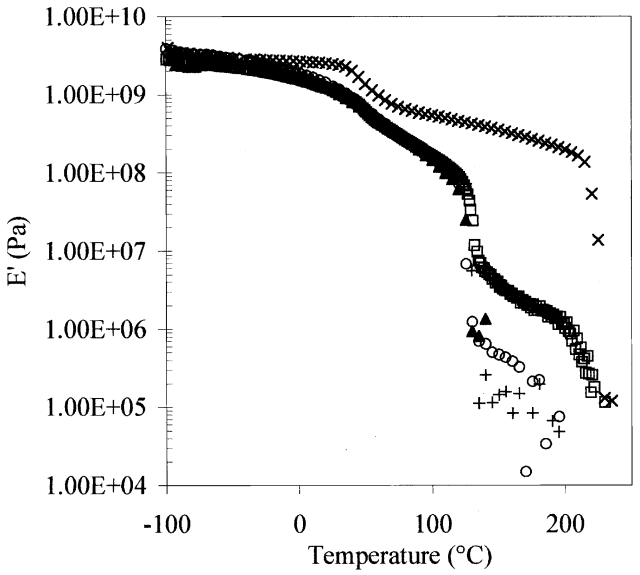

Fig. 12. Effect of temperature on the storage modulus of HDPE/PBT samples for $\lambda = 2$: HDPE (+), 10% PBT (▲), 20% PBT (○), 30% PBT (□), PBT (X)).

modulus of the matrix due to the presence of the solid substrate.

The effect of draw ratio on E' for a 56/14/30 HDPE/EVA-9/PBT is shown in Fig. 13. Again, above the melting temperature of the matrix, a plateau is observed. The results indicate that the higher the draw ratio, the higher is the storage modulus. Similar behaviour was observed by Garcia Ramirez et al. [46]. Here also the system behaves like a fibre suspension in a viscoelastic medium, the HDPE/EVA-9/PBT matrix being in the melt state and the PBT dispersed phase is in the solid state for this temperature range. This explains the behaviour observed in Fig. 13 and reported by other authors (Clark et al. [47], Ibarra et al. [48], Monleon Padras et al. [49] and Saikrasun et al. [50]. The effects of draw ratio, PBT concentration and compatibilisation on the composite for frequency sweep analysis (in the melt state) are consistent with those of temperature sweep.

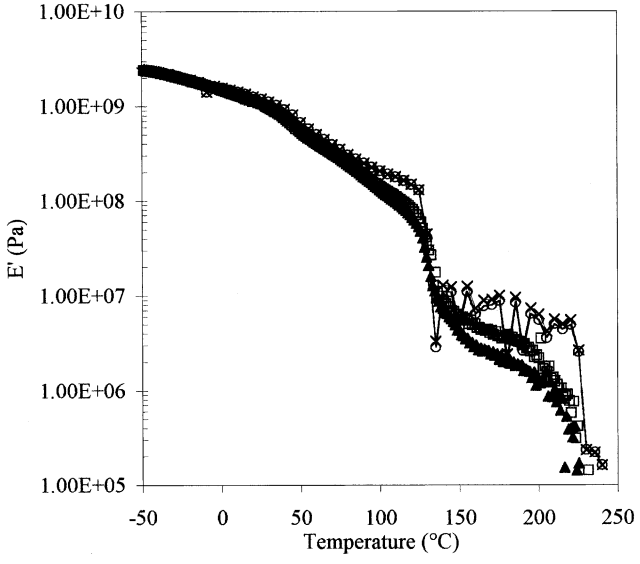

Fig. 13. Effect of draw ratio on the storage modulus of HDPE/EVA-9/PBT 56/14/30 samples — Experiments: $\lambda = 2$ (▲), $\lambda = 3.5$ (□); and model predictions (Halpin-Tsaï): $\lambda = 2$ (○), $\lambda = 3.5$ (X).

As can be seen from the above results several characteristics of the final material change, when the matrix or the draw ratio change and when the compatibilisation catalyst is present or not. In order to reduce the number of parameters and to identify the effect of the presence of EVA-9 and Bu_2SnO on the overall behaviour of the composites, we have used phenomenological models that can take into account some of the parameters that change invariably when the conditions used to obtain the in situ composites are changed. The two models are the Takayanagi model used for a draw ratio $\lambda = 1$ and the Halpin-Tsai model for $\lambda = 2$ and 3.5 for which fibrils are generated.

The Takayanagi series-parallel model consists in a mixing rule between the two limits of the series model and the parallel model [51]. For this model, the expression of the dynamic Young complex modulus of a composite (E_c^*) is given by:

$$E_c^* = E_d^* \left[\frac{(1 - \psi - \psi\phi_m)E_m^* + \psi\phi_m E_d^*}{(1 - \psi - \phi_m)E_m^* + \phi_m E_d^*} \right], \tag{1}$$

where E_d^* and E_m^* are the dynamic complex moduli of the spherical dispersed particle and the matrix, respectively. ψ stands for the volume fraction of the rigid phase, which had percolated [52]. ϕ_m is the volume fraction of the matrix. Considering ϕ_{dc} as the critical volume fraction of the dispersed phase at the percolation threshold, and b the corresponding critical exponent, ψ can be expressed in the following form of Eq. (2):

$$\psi = \phi_d \left[\frac{\phi_d - \phi_{dc}}{1 - \phi_{dc}} \right]^b \qquad \text{for } \phi_d > \phi_{dc}, \tag{2}$$

$$\psi = 0 \qquad \text{for } \phi_d < \phi_{dc},$$

where ϕ_d is the volume fraction of the dispersed phase. The critical volume fraction is defined as $\phi_{dc} = 1 - \phi_{max}$, where ϕ_{max} is the maximum packing volume fraction. The critical exponent b is around 0.4 for random sites percolation model [53,54]. Expressions of the storage and loss moduli, deduced from Eq. (2) are given by:

$$E_c' = \frac{(AC + BD)E_d' - (BC - AD)E_d''}{C^2 + D^2},$$

$$E_c'' = \frac{(BC - AD)E_d' + (AC + BD)E_d''}{C^2 + D^2}, \tag{3}$$

with:

$$A = aE'_m + bE'_d, \qquad B = aE''_m + bE''_d,$$

$$C = cE'_m + dE'_d, \qquad D = cE''_m + dE''_d$$

and with:

$$a = 1 - \psi - \psi\phi_m, \qquad b = \psi\phi_m,$$

$$c = 1 - \psi - \phi_m, \qquad d = \phi_m,$$

where E'_d, E''_d, E'_m, and E''_m are the dynamic storage and loss moduli of the spherical dispersed particles and the matrix, respectively.

ϕ_{max} depends on the particle shape and state of agglomeration. As confirmed by Fig. 4, spherical PBT particles are accompanied by PBT fibrils in a non-drawn 70/30 blend. The value of ϕ_{max} for each system is obtained by fitting model predictions to experimental data (see Fig. 13). The obtained values for ϕ_{max} are 0.7652 for HDPE matrix and 0.7656 for HDPE/EVA-9 matrix, and consequently ϕ_{dc} are, respectively, of 0.2348 and 0.2344, which are close to 0.25, value chosen by Garcia Ramirez et al. [46] for the critical volume fraction. Theoretically, for monodisperse spheres in hexagonal close packing, ϕ_{max} is 0.7405. The slight difference between the experimental and the theoretical value of ϕ_{max} are attributed to the presence of few fibrils observed for non-drawn 30% composites and also to particle dimension polydispersity. The results also indicate that EVA-9 does not have a pronounced effect on the maximum packing factor, even though the decrease of surface tension produced by the presence of EVA in the blend may have an effect on polydispersity and hence on ϕ_{max}. Overall, the model satisfactorily predicts the E' experimental data for the non-drawn samples. The fluctuations of model predictions observed at temperatures higher than the melting temperature of the matrix are due to the fluctuations of E' values of the matrix in this temperature range.

Halpin and Tsai proposed another equation for moduli, which includes the effect of the reinforcement geometry. This model was developed from elasticity calculations and demonstrates the significant effect of reinforcement geometry alone on the stiffness properties [55]. ζ, a geometry factor (see Eq. (4)), may be expressed in terms of combinations of engineering elastic constants and differences in Poisson ratios. An expression for the dynamic Young modulus of the composite (E^*_c) is given by Eq. (4), which is obtained by extending the Halpin-Tsai equation for the bulk modulus:

$$\frac{E^*_c}{E^*_m} = \frac{M_R + \zeta - \phi_d\zeta + M_R\phi_d\zeta}{M_R + \zeta - M_R\phi_d + \phi_d}, \tag{4}$$

where $M_R = E^*_d/E^*_m$ and $\zeta = 2(l/d)$, where l and d are the length and the diameter of the fibrils, respectively. E'_c and E''_c extracted from Eq. (4) are given by the following expressions:

$$E'_c = \frac{(AC + BD)E'_m - (BC - AD)E''_m}{C^2 + D^2} \tag{5}$$

$$E''_c = \frac{(BC - AD)E'_m + (AC + BD)E''_m}{C^2 + D^2}$$

with:

$$A = aE'_m + bE'_d, \qquad B = aE''_m + bE''_d,$$

$$C = cE'_m + dE'_d, \qquad D = cE''_m + dE''_d$$

and with:

$$a = \zeta(1 - \phi_d), \qquad b = (1 + \phi_d\zeta),$$

$$c = (\zeta + \phi_d), \qquad d = (1 - \phi_d).$$

It should be mentioned here that these expressions were developed for unidirectional fibre composites. Other expressions taking into account fibre orientation have also been obtained. The Halpin-Tsai model will be used with experimental data for $\lambda = 2$ and 3.5 for which fibrillation has been observed. Fig. 14 shows model predictions and experimental data of the HDPE/EVA-9/PBT 56/14/30 composites for the two draw ratios. The results indicate that the model predicts satisfactorily the experimental results up to the melt temperature of the matrix. Above this temperature, the model captures the increase of E' due to the presence of fibres but slightly overestimates the experimental data. Similar results were obtained for other PBT concentrations but are not shown here for the sake of brevity.

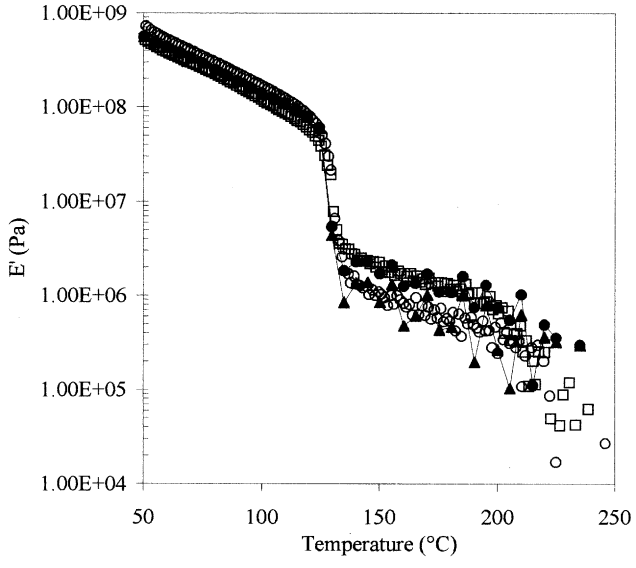

Fig. 14. Effect of matrix composition on the storage modulus of 30% PBT samples for $\lambda = 1$ — Experiments: HDPE matrix (○), HDPE/EVA-9 matrix (□) and model predictions (Takayanagi): HDPE matrix (▲); HDPE/EVA-9 matrix (●).

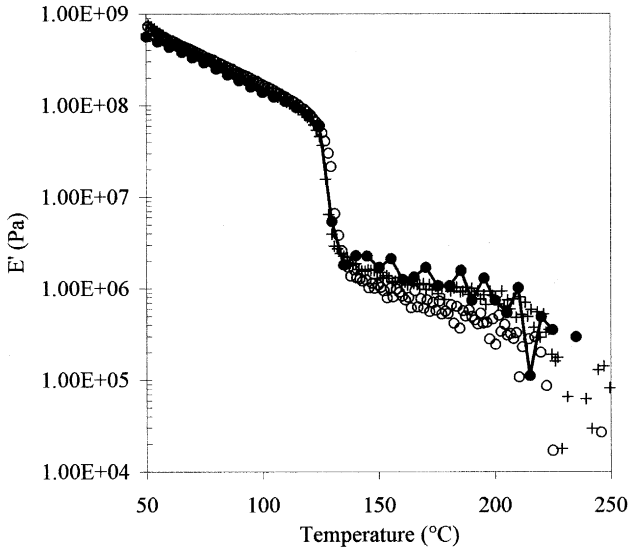

Fig. 15. Effect of matrix composition on the loss tangent of 30% PBT samples for $\lambda = 1$ — Experiments: HDPE matrix (▲), HDPE/EVA-9 matrix (●), with PBT-g-EVA-9 (■) and model predictions (Takayanagi): HDPE matrix (□); HDPE/EVA-9 matrix (X).

In the presence of the compatibiliser, E' is found to be slightly higher than that of HDPE/PBT composites (see Fig. 15). The higher values of E' can be attributed to the slight decrease of the particle diameter (see Table 2) as well as to an increase of interactions between the components due to the formation of the copolymer (see Fig. 6 and Table 3). This behaviour was also reported by Clark et al. [47], for a nylon 66/poly(vinyl pyrrolidone) glass fibre reinforced composite, and by Keush and Haessler [56] for a glass fibre reinforced epoxy. Model predictions (with the Takayanagi model) are found to be very close to the experimental results (see Fig. 15).

The moduli (E') relate to the stiffness of the material and the damping (tan δ) to the molecular motions and phase transitions. The glass transition temperature is defined as the temperature of the maximum of the loss modulus. The damping is a sensitive indicator of all kinds of molecular motions that are going on within a material. Strong fibre/matrix interactions tend to reduce the mobility of molecular chains at the interface and, therefore, reduce the damping. The low temperature range of tan δ curves, close to the glass transition of the matrix, was enlarged in order to evaluate the effect of PBT-g-EVA-9 copolymer on the mobility of the matrix chains in the presence of PBT particles [56,57]. Fig. 16a presents the results of tan δ close the glass transition of the non-drawn samples with the corresponding model predictions (Takayanagi). As expected, the presence of copolymer in the system decreases the value of tan δ (see also Table 5). This is in accordance to the work of Keush and Haessler [56] and Ibarra et al. [48], who showed that tan δ is inversely proportional to the interface bonding. The decrease observed for the EVA-9-containing is attributed to the decrease of the interfacial tension between the phases

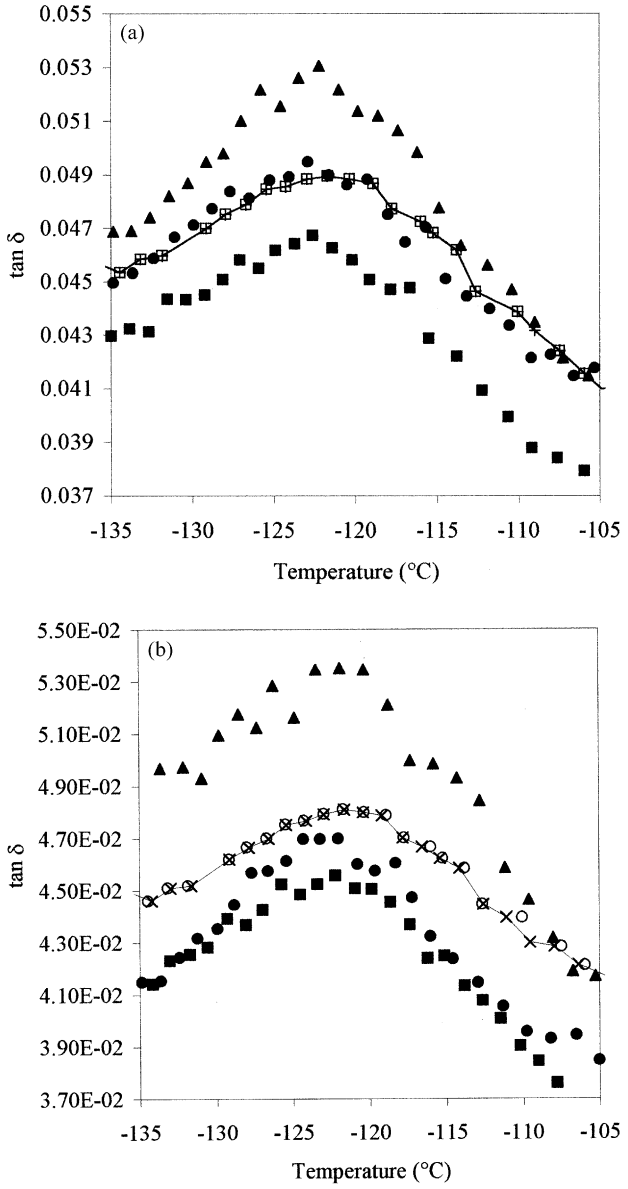

Fig. 16. (a) Effect of matrix composition on the loss tangent of 30% PBT samples for $\lambda = 1$ — Experiments: HDPE matrix (▲), HDPE/EVA-9 matrix (●), with PBT-g-EVA-9 (■) and model predictions (Takayanagi): HDPE matrix (□); HDPE/EVA-9 matrix (+). (b) Effect of matrix composition on the loss tangent of 30% PBT samples for $\lambda = 2$ — Experiments: HDPE matrix (▲), HDPE/EVA-9 matrix (●), with PBT-g-EVA-9 (■) and model predictions (Halpin-Tsai): HDPE matrix (□); HDPE/EVA-9 matrix (X).

Table 5
tan δ_{max} peaks near T_g of HDPE as a function of draw ratio (λ) and matrix composition with and without PBT-g-EVA-9 copolymer

Sample composition	tan δ_{max}
HDPE/PBT 70/30, $\lambda = 1$	0.0531
HDPE/PBT 70/30, $\lambda = 3.5$	0.0505
HDPE/EVA-9/PBT 56/14/30, $\lambda = 1$	0.0495
HDPE/(EVA-9-Bu_2SnO)/PBT 56/(13.5-0.5)/30, $\lambda = 1$	0.0467

(see Tables 4 and 5). Here again the simple addition of EVA-9 to the HDPE matrix contributes to the diminution of the interfacial tension between the matrix and the dispersed phase thereby reducing the particle diameter (see Tables 1 and 2). The predictions indicate that the model cannot capture this difference between the two samples (the slight difference of ϕ_{max} between the two samples has no effect on the predictions for tan δ. The results of Fig. 16a show that model predictions are close to the experimental results of EVA-9-containing sample. The presence of copolymer further decreases damping. This decrease is clearly attributed here to enhanced interactions between the two phases due to the presence of copolymer.

The equivalent results for $\lambda = 2$ are shown in Fig. 16b. Again, the change in the fibre aspect ratio, due to the presence of EVA-9 and EVA-9/, is relatively small to have an appreciable effect on tan δ. This indeed is clearly shown by model predictions since the same results are obtained for the different aspect ratios (see Fig. 16b). This indicates that the pronounced effect is probably due to better fibre/matrix wetting for EVA-9-containing samples. The further decrease observed in the presence of Bu_2SnO is then attributed to enhanced interactions between the constituents.

4. Conclusions

In situ organic composites with HDPE and HDPE/EVA-9 matrices and PBT dispersed phase were generated by a two step process. A compatibilisation procedure, using Bu_2SnO catalyst, was also studied on the different systems.

During the first step, the two components were melt blended at a temperature above their melting point, and drawn at the die exit. It was shown that it is possible to generate oriented PBT fibrils with draw ratios higher than one. Fibrillation was, however, possible only for PBT concentrations higher than 10% (20 and 30% in our case). The presence of the EVA-9 in the matrix contributes to a decrease in the fragmentation phenomena and to an increase in the aspect ratio of the fibrils. The rheological data in the linear viscoelasticity domain showed an increase in the storage modulus, G', as the PBT concentration increases. An increase was also found when the draw ratio is increased, in the presence of the EVA-9 in the matrix and in the presence of the generated copolymer. For 30% PBT composites, a pseudo equilibrium plateau is observed in the low-frequency range and is attributed, as in other multiphase systems, to interparticular interactions. This plateau is found to increase with the addition of EVA-9 and with the copolymer generation. Dynamic mechanical analysis indicated that the presence of the fibrils in the composite increases the modulus at temperatures higher than the melting temperature of the matrix. The presence of the generated copolymer slightly increases the values of the dynamic modulus (E'). It also contributes to a decrease of the damping close to the glass transition of the matrix. This is attributed to a lower molecular mobility due to better interactions between the phases. Quantitative analysis using Takayanagi and Halpin-Tsai models highlighted the effects of draw ratio, matrix composition and copolymer on the storage modulus of composites.

Results of mechanical properties (tensile and impact) for this particular system were not very conclusive (Boyaud [58]). These results are not presented here for the sake of brevity. However, experimental results on PP/PA in situ composites, prepared in a way similar to that presented in this work, indicate that, depending on the processing conditions and the concentration of PA in PP matrix, tensile modulus higher than that of the constituents (PP and PA) can be obtained for composites (Pesneau et al. [59]). More experimental work is needed in the case of HDPE/PBT systems.

Acknowledgements

The authors acknowledge the financial support provided by the Natural Sciences and Engineering Research Council (NSERC) of Canada and the Fonds pour la Formation de chercheurs et l'aide à la recherche (FCAR) of the province of Quebec.

References

[1] Kiss G. Polym Eng Sci 1987;27:410.
[2] Dutta D, Fruitwala H, Kohli A, Weiss RA. Polym Engng Sci 1990;30:1005.
[3] Chinsirikul W, Hsu TC, Harrison IR. Polym Eng Sci 1996;36:2708.
[4] La Mantia FP, Geraci C, Vinci M, Pedretti U, Roggero A, Minkova LI, Magagnini PL. J Appl Polym Sci 1995;58:911.
[5] Crevecoeur G, Groeninckx G. J Appl Poym Sci 1993;49:839.
[6] Champagne MF, Dumoulin MM, Utriacki LA, Szabo JP. Polym Engng Sci 1996;36:1636.
[7] Carafagna C, Amendola E, Nicolais L. Int J Mater Product Technol 1992;7:205.
[8] Magagnini PL, Paci M, Minkova LI, Miteva TS, Sek D, Grobelny J, Kaczmarczyk B. J Appl Polym Sci 1996;60:1665.
[9] Wong SC, Mai YW, Leng Y. Polym Eng Sci 1998;38:156.
[10] Mehta S, Deopura BL. J Appl Polym Sci 1995;56:169.
[11] Sabol EA, Handlos AA, Baird DG. Polym Compos 1995;16:330.
[12] Heino M. Chem Technol Metall Ser 1994;220:1.
[13] Datta A, Baird DG. Polymer 1995;36:505.
[14] Evstatiev M, Nicolov N, Fakirov S. Polymer 1996;37:4455.
[15] Evstatiev M, Schultz JM, Petrovich S, Georgiev G, Fakirov S, Friedrich KJ. J Appl Polym Sci 1998;67:723.
[16] Apostolov AA, Falirov S, Sezen B, Bahar I, Kloczkowski A. Polymer 1994;35:5247.
[17] Fakirov S, Evstatiev M, Schultz JM. Polymer 1993;34:4669.
[18] Apostolov AA, Evstatiev M, Fakirov S, Kloczkowski A, Mark JE. J Appl Polym Sci 1996;59:1667.
[19] Li X, Chen M, Huang Y, Cong G. Polym J 1997;29:975.
[20] Monticciolo A, Cassagnau P, Michel A. Polym Engng Sci 1998;38:1882.
[21] Pesneau I, Aït-Kadi A, Bousmina, M, Cassagnau P, Michel A. ANTEC 99. New York, May 2–6 1999;2661.

[22] Pesneau I, Aït-Kadi A, Bousmina M, Cassagnau P, Michel A. Colloque bisannuel GFP/SQP, Ste-Adèle (Québec), May 1999;9–11.
[23] Utracki LA. Polymer alloys and blends. New York: Hanser, 1989.
[24] Gimenez J, Boudris M, Cassagnau P, Michel A. Polym Reaction Eng 2000;8(2):135–57.
[25] Gimenez J, Boudris M, Cassagnau P, Michel A. Int Polym Process 2000;15(1):20–7.
[26] Pesneau I, Llauro M-F, Grégoire M, Michel A. J Appl Polym Sci 1997;65:2457.
[27] Legros A, Carreau PJ, Favis BD, Michel A. Polymer 1997;38:5085.
[28] Pesneau I. Thesis, Université Claude-Bernard Lyon I, 1997.
[29] Mack WA. Chem Engng 1972;May 15:99.
[30] Todd DB. Chem Engng Process 1992;August:72.
[31] Bonetti J. Thesis, Université Claude Bernard Lyon I, 1992.
[32] Espinasse I, Pétiaud R, Llauro M-F, Michel A. Int J Polym Anal Characterisation 1995;1:137.
[33] Grace HP. Chem Eng Commun 1982;14:225.
[34] Taylor GI. Proc R Soc 1934;A-146:501.
[35] Moroni A, Casale A. In: Proceedings of the Seventh International Congress of Rheology, 1976;339.
[36] Münstedt H. Polym Engng Sci 1981;21:259.
[37] Aoki Y. Macromolecules 1987;20:2208.
[38] Bousmina M, Müller R. J Rheol 1993;37:663.
[39] Bousmina M, Müller R. Rheol Acta 1996;35:369.
[40] Carreau PJ, Bousmina M, Ajji A. Pacific polymers. New York: Springer, 1994. p. 25.
[41] Aranguren MI, Mora E, DeGroot Jr. JVM, Macosko CW. J Rheol 1992;36:1165.
[42] Otsubo Y. Theoretical and Applied Rheology. vol. 2. Bruxelles, 17–21 August 1992;628.
[43] Aoki Y, Nakayama K. Polym J 1982;14:951.
[44] Ferry JD. Viscoelastic properties of polymers. 3rd ed. New York: Wiley, 1987.
[45] Boyaud M.-F, Aït-Kadi A, Bousmina M, Michel A, Cassagnau P. Polym Engng Sci. 2001.
[46] Garcia Ramirez M, Cavaillé JY, Dufresne A, Tékély P. J Polym Sci 1995;33:2109.
[47] Clark Jr. RL, Craven MC, Kander RG. Composites 1999;A-30:37.
[48] Ibarra L, Macìas A, Palma E. J Appl Polym Sci 1995;57:831.
[49] Moleon Padras M, Schaber G, Gomez Ribelles JLG, Romeo Colomer FR. Macromolecules 1997;30:3612.
[50] Saikrasun S, Amornsakchai T, Sirisinha C, Meesiri W, Bualek-Limcharoen S. Polymer 1999;40:6437.
[51] Takayanagi M, Uemura S, Minami S. J Polym Sci 1964;5:113.
[52] Ouali N, Cavaillé JY, Perez J. Pl Rub Comp Proc Appl 1991;16:55.
[53] de Gennes PG. Scaling concepts in polymer physics. Ithaca, New York: Cornell University Press, 1979.
[54] Stauffer D. Introduction to percolation theory. London: Taylor and Francis, 1985.
[55] Halpin JC, Kardos JL. Polym Engng Sci 1976;16:344.
[56] Keusch S, Haessler R. Composite: Part A 1999;30:997.
[57] Pegoretti A, Della Volpe C, Detassis M, Migliaresi C. Composite: Part A 1996;27:1067.
[58] Boyaud M-F. MSc Thesis, Laval University, 2000.
[59] Pesneau I, Aït-Kadi A, Bousmina M, Cassagnau P, Michel A. in preparation for Polymer, 2001.